

# Growing and decaying processes and resistance of sand waves in the vicinity of the Tone River mouth

S. Okamura

IDEA Consultants, Inc., Tokyo, Japan

S. Fukuoka

Chuo University, Tokyo, Japan

**ABSTRACT:** The long-term growth and decay processes and resistance of sand waves of the Tone River mouth from 1961 to 2007 are clarified in this paper. At first, we examine characteristics of the arrangement of dunes which are seen in the downstream of the Choshi Ohashi Bridge. Next, the long-term growth and decay processes of dunes are indicated by the variation of cross-sectional bed forms surveyed from 1961 to 2007. The variation of sand waves resistances and bed elevations during the floods in different years is evaluated by a numerical unsteady flood flow and bed variation analysis based on the observed temporal changes in water surface profiles. At last, characteristics of the sand wave resistances in the Tone River mouth are clarified by comparing with the previous studies on sand wave resistances in alluvial rivers.

## 1 INTRODUCTION

### 1.1 Flood flow and sediment movement analysis system

For river management, it is important to estimate the bed variations during floods and the resistances in flood flows including sand waves resistances.

To figure out flood flows and bed variations during floods, Fukuoka (2011) proposed the flood flow and sediment movement analysis system based on the observation of temporal changes in water surface profiles shown in Figure 1. This

system is based on the idea that the influences of channel shape, resistance, bed variation and so on are reflected in temporal changes in water surface profiles of flood flows.

In the system, temporal changes in water surface profiles and discharge hydrographs during the period of floods and bed elevations before and after floods are observed at the sections in question. Then, we can figure out flood phenomena by computing the unsteady flood flow and bed variation so as to explain these observed data.

In this paper, we apply the system to the vicinity of the Tone River mouth in order to estimate the bed variations and the resistances of sand waves during floods.

### 1.2 Problem of the Tone River mouth

The rise of water level during floods in the Tone River mouth is remarkable and brings a problem of flood inundation near the river. But the reason why the water rise and the steep water surface gradient near the river mouth was generated has not yet been explained.

In this paper, we indicate that the sand waves are formed in the vicinity of the Tone River mouth and cause the rise of water level during floods. Then, the long-term growth and decay processes of sand waves and the variations of sand waves resistances are clarified by the relation with bed variations of the Tone River mouth from 1961 to 2007.

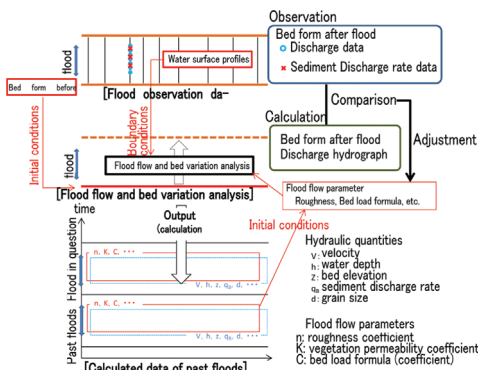


Figure 1. Flood flow and sediment movement analysis system based on the observation of temporal changes in water surface profiles.

The variations of sand waves resistances and bed elevations during floods in different years are evaluated by a numerical unsteady flood flow and bed variation analysis based on the observed temporal changes in water surface profiles. At last, the characteristics of the sand wave resistances in the Tone River mouth are clarified by comparing with the previous studies on sand wave resistances in alluvial rivers.

## 2 THE BED FORM IN THE TONE RIVER MOUTH

### 2.1 Bed material grain size

Figure 2 shows the planer distribution of grain size of bed material in the surface layer. Whereas the bed material is composed of silt or sand in most areas around the river mouth, the gravel component dominates from  $-1.0$  km to  $0.5$  km section, where the channel width is decreased by the training dikes. Figure 3 shows the vertical

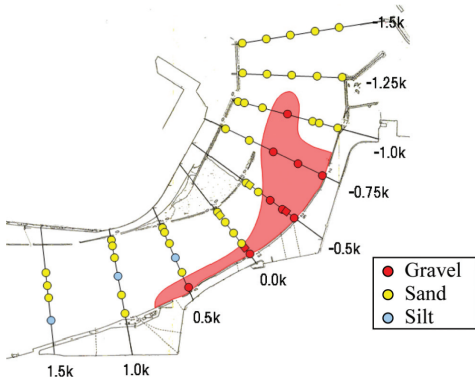


Figure 2. Planer distribution of bed material.

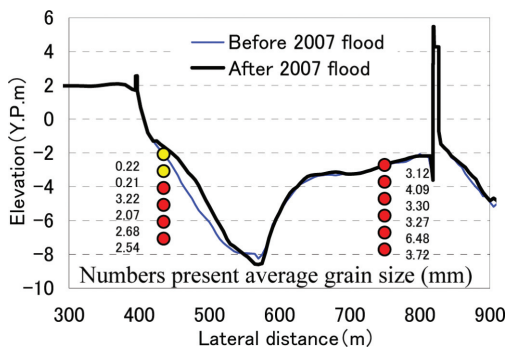


Figure 3. Vertical profiles of average grain size of  $-0.5$  k cross-section.

profiles of average grain size surveyed at left and right side of  $-0.5$  km cross-section. The comparison of cross-sectional bed form before and after 2007 flood is also shown in Figure 3. At the left side, although the sand exists in surface layer, the gravel exists in lower layer. At the right side, the gravel exists from river bed to the depth of about  $5$  m from river bed. The river bed elevation at the right side of  $-0.5$  km cross-section is maintained due to the gravel bed materials even though there are located at the outer side of the narrow curved channel.

### 2.2 Distribution of sand waves

Figure 4 shows the plan form and bed elevations of the Tone River mouth. Bed elevations are surveyed at  $50$  m intervals in 2003 and  $20$  m intervals in 2009 longitudinally. Figure 5 shows the longitudinal bed forms along the channel center line shown in Figure 4. While the undulation of bed form is mild from  $6$  km to  $10$  km section, the bed form in the downstream of  $6$  km section is rugged. The sand waves are considered as dunes for the following reason. The water depth of the section is from  $5$  m to  $10$  m during floods. Generally, the wave length and wave height of the dune estimated about ten times longer than the water depth and from one-fifth to one-tenth of the water depth, respectively.

### 2.3 Sand waves in the downstream of the Choshi Ohashi Bridge

Figure 6 shows planer distribution of bed elevations of downstream of the Choshi Ohashi Bridge (located in the reach  $2.25$  km upstream from the river mouth) where the large dunes can be seen. The dashed lines pass through the wave tops of dunes in the figure. The arrangements of dunes are fish-scale pattern.

Kinoshita (1984) found that longitudinal vortices are often seen and the sand waves often form fish-scale pattern at downstream of bridge piers. He indicated that stable longitudinal vortices emerge when the cross-sectional intervals of dunes are four times wider than the water depth by the channel experiment.

Figure 7 shows the cross-sectional bed forms at  $1.5$  km upstream from the river mouth and the Choshi Ohashi Bridge ( $2.25$  km). The cross-sectional intervals of dunes (about  $20$  m) are four times wider than the water depths during floods (about  $5$  m). The arrangement of dunes which are seen in the downstream of the Choshi Ohashi Bridge verified it to be scale-like dunes as Kinoshita found.

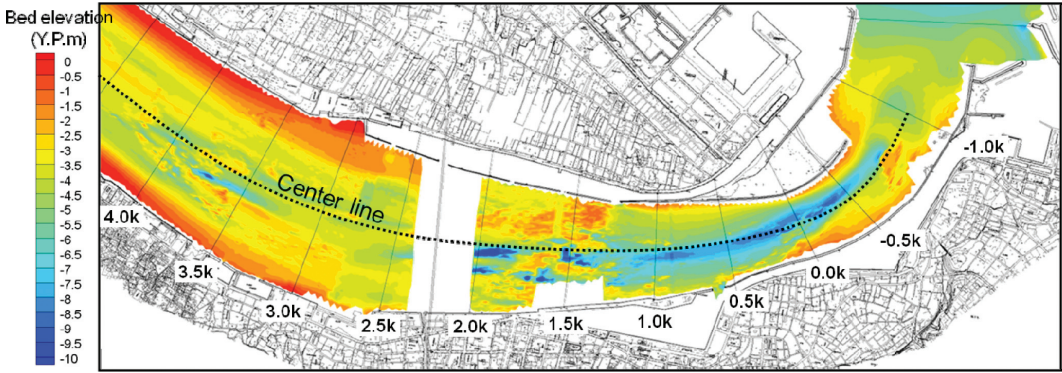


Figure 4. Plan form and surveyed bed elevation of the Tone River mouth.

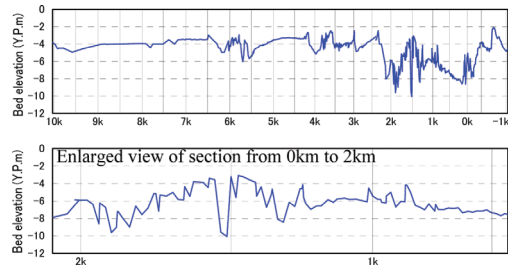


Figure 5. Longitudinal bed forms along the center line.

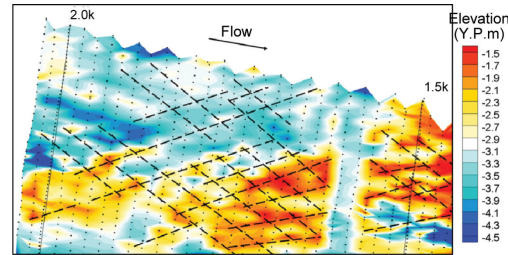


Figure 6. Scale-like dunes in the downstream of the Choshi Ohashi Bridge.

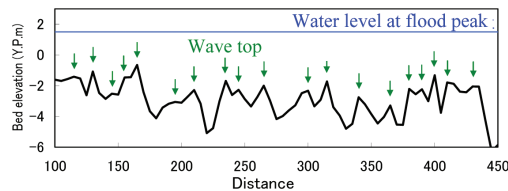


Figure 7(a). Cross-sectional bed form at Choshi Ohashi Bridge.

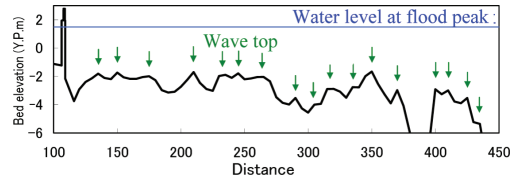


Figure 7(b). Cross-sectional bed form at 1.5 km.

### 3 GROWTH AND DECAY PROCESSES OF SAND WAVES FROM 1961 TO 2007

In this section, we examine the growth and decay processes of the sand waves with the cross-sectional surveying data which were started in 1961.

Figure 8 shows the peak discharge of floods over 3,000 m<sup>3</sup>/s and the years when the cross-sectional bed forms were surveyed.

The floods over 6,000 m<sup>3</sup>/s didn't occur in the 1960's and 1970's. Floods came in groups in the three years from 1981 to 1983. There are many floods over 6,000 m<sup>3</sup>/s after 1998.

Figure 9(a)–9(d) show the changes of cross-sectional bed forms in the reach downstream of 6.5 km from 1961 to 2007. In these Figures, small bumps existing on the bed surfaces are dunes. From these Figures, the growth and decay processes of the sand waves are clarified as follows.

The sand waves whose heights are from 1 m to 2 m had existed on many cross-sections before 1965 as shown in Figure 9(a). But most of them disappeared with sediment deposition in the river mouth area from 1965 to 1970 and the cross-sectional bed forms became smooth. Dredges were concentrated in this age in the section from 20 km to 40 km (Moro et al., 2011). It is thought that the fine sediments yielded with dredging in

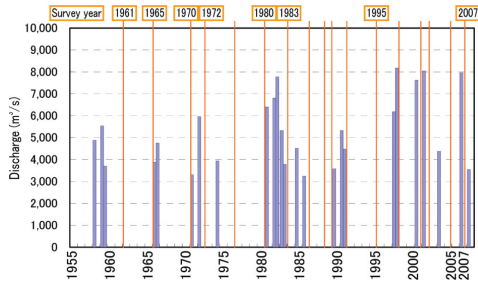


Figure 8. Peak discharge of floods and the years when the cross-sectional bed forms were surveyed.

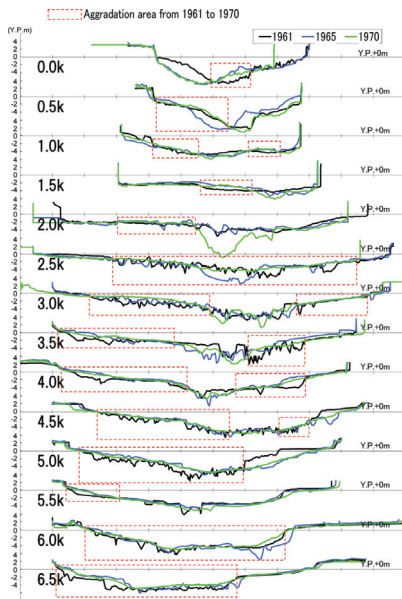


Figure 9(a). Variation of cross-sectional bed forms from 1961 to 1970.

the upstream section deposited in the reach downstream of 6.0 km from river mouth.

The bed elevations are stable and the sand waves cannot be seen from 1970 to 1980 as shown in Figure 9(b). In this period, large flood didn't occur except 1947.

After that, the sand waves grew again from 1980 to 1983 as shown in Figure 9(c). In this period, a number of large floods occurred and the bed elevations degraded about 0.5 m–1.0 m in the entire section of river mouth.

After 1983, the height and the distribution area of the sand waves have grown gradually up to 2007 as shown in Figure 9(d).

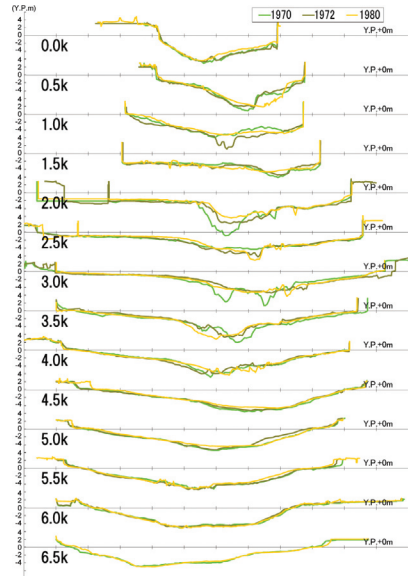


Figure 9(b). Variation of cross-sectional bed forms from 1970 to 1980.

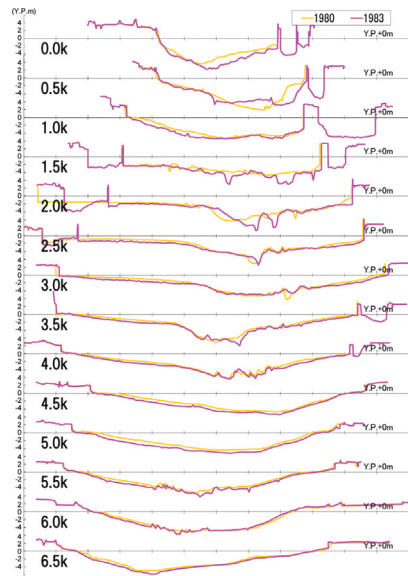


Figure 9(c). Variation of cross-sectional bed forms from 1980 to 1983.

As above, in the reach downstream of 6.0 km from the Tone River mouth, although the sand waves had existed in the 1960's, most of them disappeared with sediment deposition in the river mouth area in the 1970's. After that, the sand waves grew

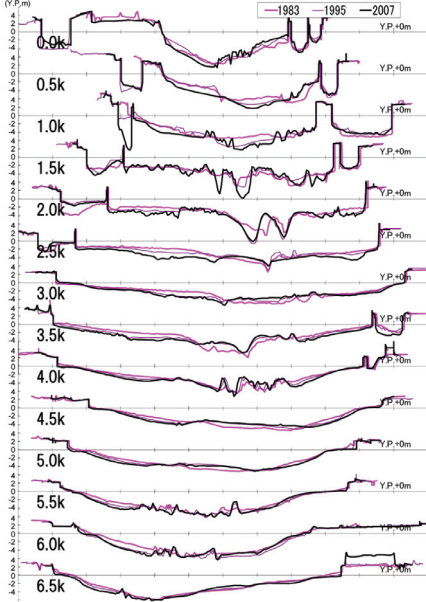


Figure 9(d). Variation of cross-sectional bed forms from 1983 to 2007.

again with the degradation of bed elevation caused by a series of floods from 1981 to 1983. Then the height and the distribution area of the sand waves have grown gradually up to the present date.

#### 4 THE VARIATION OF SAND WAVE RESISTANCES AND BED ELEVATIONS DURING THE FLOODS

We apply the flood flow and sediment movement analysis system based on the observation of temporal changes in water surface profiles to the floods in different years of the Tone River in order to evaluate the variation of sand wave resistances and bed elevations during the floods with growth and decay processes of sand waves.

##### 4.1 Computational method and conditions

We develop unsteady numerical analyses by solving the flows and bed variations during the floods in different years so as to coincide with observed temporal changes in water surface profiles. The discharge hydrograph and bed forms after the flood are compared with observed data.

The analysis consists of quasi-3D unsteady flow analysis (Uchida and Fukuoka, 2009) as shown in Eqs. (1)–(3) and 2D bed variation analysis for graded sediment (Fukuoka et al., 1998), employing

the general coordinate system. The bed load is calculated by the formula of Fukuoka (2010).

In the quasi-3D unsteady flow analysis, the horizontal velocity  $u_i$  at  $\zeta = (z_s - z)/h$  is assumed as shown in Eq. (1). Where  $i, j = x, y$ ,  $\delta u_i$  is the difference between depth averaged velocity  $U_i$  and bottom velocity  $u_{bi}$ .  $\delta u_i$  is calculated by Eq. (2) using depth integrated vorticity  $\Omega_i$ .

$$u_i - U_i = \frac{\delta u_i}{2} (1 - 3\zeta^2) \quad (1)$$

$$\delta u_i = U_i - u_{bi} = \frac{2}{3} \left( \varepsilon_{ij3} \Omega_j h - \frac{\partial W h}{\partial x_i} \right) \approx \frac{2}{3} \varepsilon_{ij3} \Omega_j h \quad (2)$$

where spatial change of depth averaged vertical velocity  $W$  is assumed to be negligible in shallow flows. Depth averaged horizontal velocity  $U$  is calculated by shallow water equations employing the general coordinate system  $(\xi, \eta)$ .

$\Omega_i$  is calculated by horizontal vorticity equation as shown in Eq. (3).

$$\begin{aligned} \frac{\partial J h \Omega_i}{\partial t} + \frac{\partial h \Delta \eta (F_{i\xi} + D_{i\xi})}{\partial \xi} + \frac{\partial h \Delta \xi (F_{i\eta} + D_{i\eta})}{\partial \eta} \\ = J (ER_{-i} + P_{oi}) \end{aligned} \quad (3)$$

where  $F_{i\xi}, F_{i\eta}$  = flux of  $\Omega_i$  with expansion, contraction and rotation,  $D_{i\xi}, D_{i\eta}$  = flux of  $\Omega_i$  with diffusion,  $ER_{-i}$  = rotation term,  $P_{oi}$  = production term.

The concentration of suspended sediment is calculated by 3D advection-diffusion equations (Okamura and Fukuoka, 2012) as shown in Eq. (4). Where, the velocities are calculated by quasi-3D unsteady flow analysis. This analysis can calculate vertical distribution of suspended sediment concentration due to secondary flow.

$$\begin{aligned} \frac{\partial c_k}{\partial t} + \frac{1}{J} \left( \frac{\partial \Delta \eta \cdot u^\xi c_k}{\partial \xi} + \frac{\partial \Delta \xi \cdot u^\eta c_k}{\partial \eta} \right) \\ + \frac{\partial c_k (u^\sigma - \sigma_t - w_{0k})}{\partial \sigma} \\ = \frac{\partial}{\partial \xi} \left( \varepsilon_s \cdot \frac{\partial c_k}{\partial \xi} \right) + \frac{\partial}{\partial \eta} \left( \varepsilon_s \cdot \frac{\partial c_k}{\partial \eta} \right) \\ + \cos \theta^\xi \left\{ \frac{\partial}{\partial \xi} \left( \varepsilon_s \cdot \frac{\partial c_k}{\partial \eta} \right) + \frac{\partial}{\partial \eta} \left( \varepsilon_s \cdot \frac{\partial c_k}{\partial \xi} \right) \right\} \\ + \frac{\varepsilon_s}{J} \left\{ \frac{\partial c_k}{\partial \xi} \frac{\partial \theta^\xi}{\partial \eta} + \frac{\partial c_k}{\partial \eta} \frac{\partial \theta^\eta}{\partial \xi} \right\} + \frac{\partial}{\partial z} \left( \varepsilon_s \cdot \frac{\partial c_k}{\partial z} \right) \\ + q_{suk} \end{aligned} \quad (4)$$

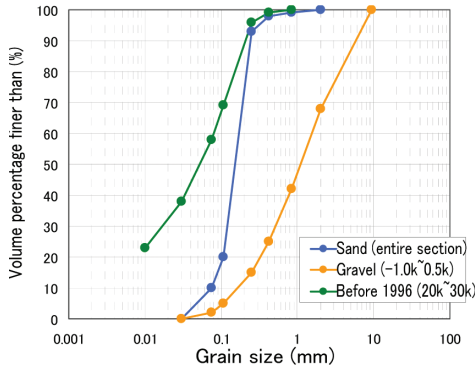


Figure 10. Initial grain size distributions in the simulation.

where  $c_k$  = concentration of suspended sediment of  $d_k$  (arbitrary grain diameter),  $w_{0k}$  = falling velocity of grain,  $\varepsilon$  = coefficient of diffusion. Pick up rate of suspended sediment from bed surface ( $q_{stak}$ ) is calculated by the formula of Itakura and Kishi (1980).

The boundary conditions of upstream and downstream ends are defined as observed water levels around 30 km point and astronomical tide levels of the Choshi tidal observatory at sea of 4 km from the river mouth, respectively. Figure 10 shows initial grain size distributions.

We evaluate the resistance of flood flows using the Manning's roughness coefficient including sand wave resistances. The section in question is divided in three subsections. The bed material is composed of gravel in the subsection from -1.0 km to 0.5 km. The sand waves exist in the subsection from 0.5 km to 6.0 km. Sand waves don't exist and the bed material is composed of sand in the subsection upstream of 6.0 km. The Manning's roughness coefficients are determined so as to minimize the differences between the observed and the calculated water surface profiles in each subsection, respectively.

#### 4.2 Computation of the September 2007 flood

Figure 11 shows locations of observation stations of water levels and discharge to 30 km from the river mouth. Temporal data of water levels were measured at many observation stations. Figure 12 shows observed water level hydrographs of the September 2007 flood. The flood peak occurred in the stage of low tide.

The observed temporal changes in water surface profiles are accurately reproduced by deciding the Manning's roughness coefficient  $n = 0.028$  from -1.0 km to 6.0 km section where the sand waves exist and  $n = 0.014$  upstream from 6.0 km, respectively as shown in Figure 13.

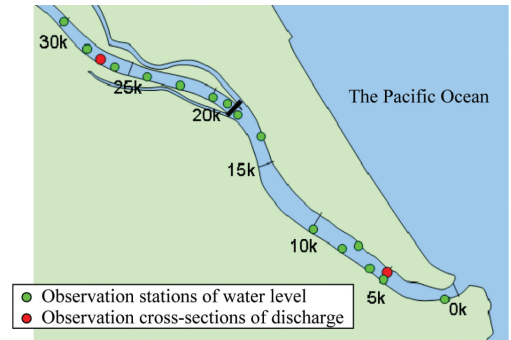


Figure 11. Observation stations during the 2007 flood.

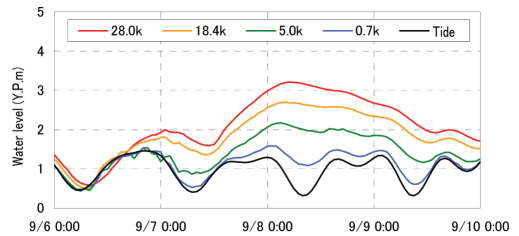


Figure 12. Observed water level hydrographs of the September 2007 flood.

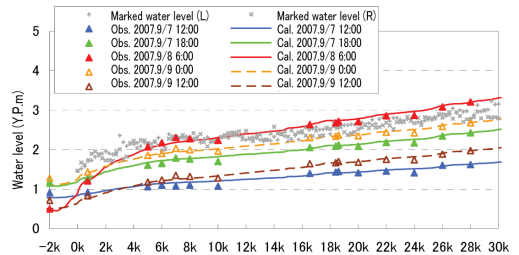


Figure 13. Comparison between observed and calculated water surface profiles during the September 2007 flood.

Figure 14 shows the comparison of observed and calculated bed elevation before and after the flood. The calculated bed variation is similar to observed bed variation. The bed elevation is maintained in most parts of the section and decreases about 0.5 m at 0.0 km point.

The calculated discharge hydrograph corresponds with the observed discharge hydrograph as shown in Figure 15.

As above, high resistances due to sand waves appeared to act on the flood flow in the section downstream of 6.0 km from river mouth.

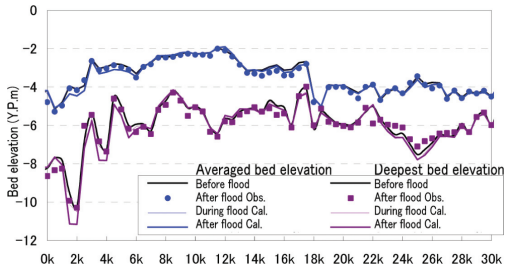


Figure 14. Comparison between observed and calculated bed elevation before and after the September 2007 flood.

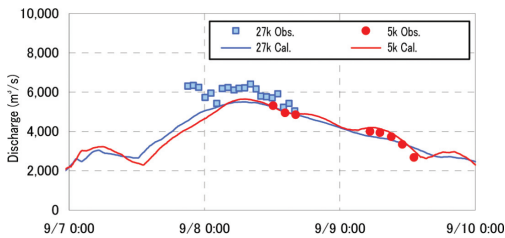


Figure 15. Comparison between observed and calculated discharge hydrographs.

### 4.3 Computation of the 1981~1983 floods

The sand waves grew again with the bed degradation caused by a series of floods from 1981 to 1983. Figure 16 shows observed water level hydrographs of the floods from 1981 to 1983.

Figure 17 shows the comparison between temporal changes in observed and calculated water surface profiles during the September 1982 flood. Although the numbers of the water level measurement points are not so many, the results of the analysis correspond with temporal changes in observed water surface profiles during the flood. Where the Manning's roughness coefficient  $n = 0.022$  from  $-1.0$  km to  $0.5$  km section,  $n = 0.016$  from  $0.5$  km to  $6.0$  km section and  $n = 0.012$  upstream from  $6.0$  km. The Manning's roughness coefficient is smaller than that of the 2007 flood in the section downstream of  $6.0$  km. Temporal changes in observed water surface profiles of other floods occurred in the period from 1981 to 1983 are re-created by the same conditions of Manning's roughness coefficients as shown in Figure 18.

Figure 19 shows the changes in averaged bed elevations and deepest bed elevations from 1980 to 1983. The solid lines indicate the calculated bed elevations after the each flood. Bed elevations degraded every flood. The calculated bed

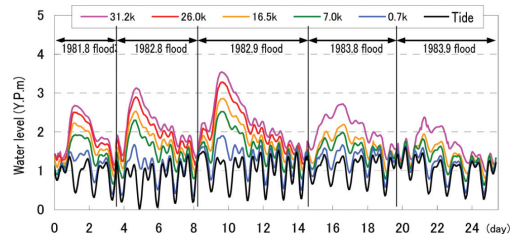


Figure 16. Observed water level hydrographs of the floods from 1981 to 1983.

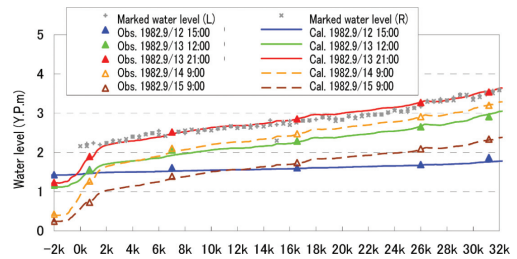


Figure 17. Comparison between temporal changes in observed and calculated water surface profiles during the September 1982 flood.

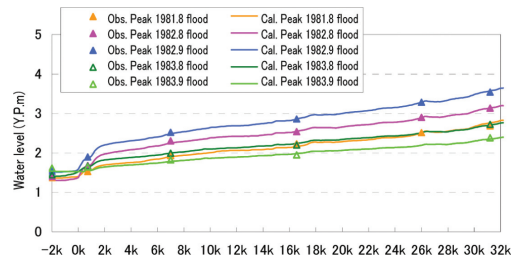


Figure 18. Comparison between observed and calculated peak water surface profiles during the floods from 1981 to 1983.

elevations after the September 1983 flood explain well the observed bed elevations.

Figure 20 shows the observed and the calculated contours of bed variations from 1980 to 1983. Calculation results explain the bed degradation caused by a series of floods from 1981 to 1983.

The calculated discharge hydrographs correspond with the observed discharge hydrographs as shown in Figure 21.

### 4.4 Computation of the September 1972 flood

The September 1972 flood occurred after most of sand waves disappeared with sediment deposition in the river mouth area from 1965 to 1970.

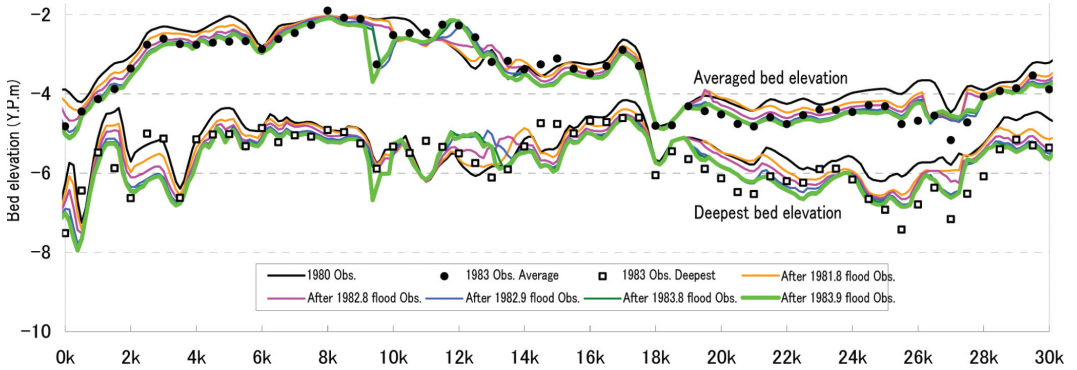


Figure 19. Comparison between observed and calculated bed elevation before and after the floods from 1981 to 1983.

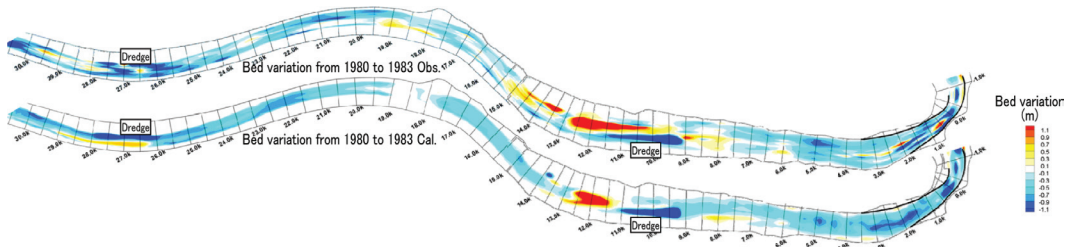


Figure 20. Observed and the calculated contour of bed variations from 1980 to 1983.

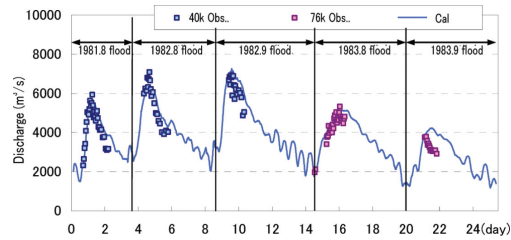


Figure 21. Comparison between observed and calculated discharge hydrographs of the floods from 1981 to 1983.

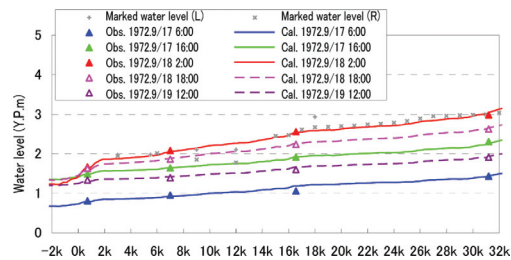


Figure 22. Comparison between observed and calculated water surface profiles during the September 1972 flood.

Figure 22 show the comparison between temporal changes in observed and calculated water surface profiles during the September 1972 flood. Temporal changes in calculated water surface profiles correspond with observed ones, where the Manning's roughness coefficient is  $n = 0.012$  in the entire section in question. This value of Manning's roughness coefficient is almost equal to the resistance on flat bed.

Figure 23 show the comparison between observed and calculated discharge hydrographs.

The differences of bed elevations before and after the flood are smaller than 0.5 m both in calculation and observation as shown in Figure 24.

#### 4.5 Computation of the August 1959 flood

The sand waves had existed on many cross-sections before 1965.

Figure 25 shows the comparison of temporal changes in observed and calculated water surface profiles during the August 1959 flood. The Manning's roughness coefficient was  $n = 0.020$  from  $-1.0$  km to  $6.0$  km section and  $n = 0.013$  upstream from  $6.0$  km. Temporal changes in calculated water surface profiles correspond with

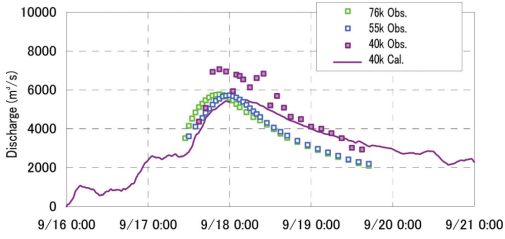


Figure 23. Comparison between observed and calculated discharge hydrographs of the September 1972 flood.

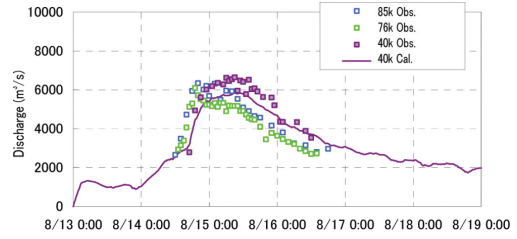


Figure 26. Comparison between observed and calculated discharge hydrographs of the September 1959 flood.

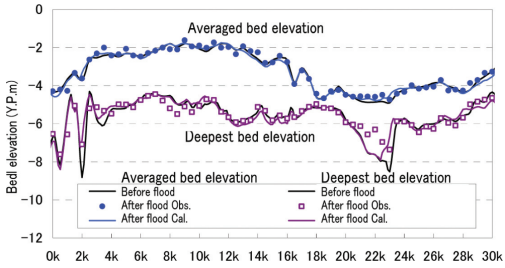


Figure 24. Comparison between observed and calculated bed elevation before and after the September 1972 flood.

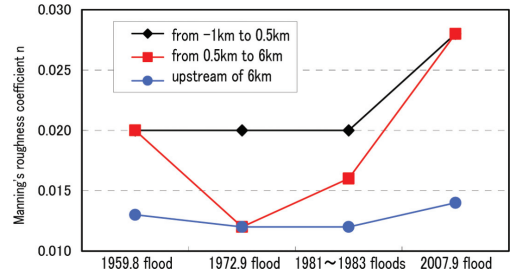


Figure 27. Long-term variations of the Manning's roughness coefficients in each section.

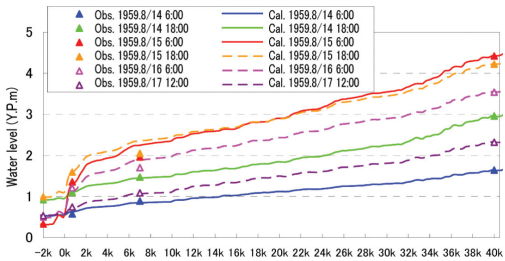


Figure 25. Comparison between observed and calculated water surface profiles during the September 1959 flood.

observed ones in flood rising period (before 8/14 18:00) and flood falling period (after 8/17 12:00). But calculated water surface profiles are higher than observed ones in flood peak (8/15 6:00~8/16 6:00). The bed resistance could have changed during the flood, but it's not sure whether is insufficient of observation data of water level. The bed variations during the flood are not clear, because the cross-sectional bed forms had not been surveyed till before 1961.

Figure 26 shows the comparison between observed and calculated discharge hydrographs.

It is presumed that the Manning's roughness coefficient would have been  $n = 0.020$  in the reach downstream of 6.0 km except the flood peak.

#### 4.6 Long-term variation of sand wave resistances

Figure 27 shows long-term variations of the Manning's roughness coefficients in each section which were evaluated by the unsteady flood flow and bed variation analysis based on the observed temporal changes in water surface profiles from 1959 to 2007. In the section upstream of 6.0 km where the sand waves have not been existed, the Manning's roughness coefficients are  $n = 0.012\sim 0.014$  in every flood. They are usual value of Manning's roughness coefficients in the vicinity of river mouth. In the section from  $-1.0$  km to 0.5 km where the bed material is composed of gravel, the Manning's coefficients are high value  $n = 0.020\sim 0.028$  in every flood.

On the other hand, in the section from 0.5 km to 6.0 km, the Manning's roughness coefficients have changed with the long-term growing and decaying processes of sand waves. The Manning's roughness coefficient was  $n = 0.020$  when the sand waves had existed except the peak of the August 1959 flood. The roughness coefficient became small ( $n = 0.012$ ) in the September 1972 flood which occurred after

most of sand waves disappeared with sediment deposition in the river mouth. After that, the roughness coefficient increased a little bit ( $n = 0.016$ ) in a series of floods from 1981 to 1983 when the sand waves grew again. Then the roughness coefficient became large ( $n = 0.028$ ) in the September 2007 flood the height and the distribution area of the sand waves have grown up.

## 5 RESISTANCE OF SAND WAVES IN THE VICINITY OF THE TONE RIVER MOUTH

There have been a lot of researches on the resistance of sand waves introducing the “effective bed shear stress” in order to discuss the resistance of sand waves since Einstein and Barbarossa (1952). In this section, we attempt to describe the resistances in the Tone River mouth calculated by the quasi-three dimensional unsteady flow and bed variation analysis by one dimensional quantities. Then the resistances in the Tone River mouth are compared with the results of previous researches on the resistance of sand waves studied in one dimensional analysis.

### 5.1 Previous researches on the resistance of sand waves

Einstein and Barbarossa (1952) tried to estimate the resistance of sand waves dividing the total resistance into the friction resistance and the form resistance as shown below.

$$R = R' + R'', u_* = u_*' + u_*'' \quad (5)$$

$$u_*' = (gR'I)^{1/2}, u_*'' = (gR''I)^{1/2} \quad (6)$$

$$u/u_*' = 5.75 \log(12.2R'x/k_s) \quad (7)$$

where,  $R$  = hydraulic radius,  $R'$  = hydraulic radius related to the friction resistance,  $R''$  = hydraulic radius related to the form resistance,  $u$  = velocity,  $u_*$  = shear velocity,  $g$  = gravity acceleration,  $I$  = energy gradient,  $x$  = coefficient,  $k_s$  = equivalent roughness.

Engelund (1967) also investigate the resistances in alluvial rivers and the experimental channels basing on the “effective bed shear stress”. Engelund indicated that the total bed shear stress  $\tau_*$  was a function of the effective bed shear stress  $\tau_*'$  by the data of experimental channels.

$$\tau_* = RI/sd, \tau_*' = R'I/sd \quad (8)$$

$$\frac{u}{\sqrt{gR'I}} = 6.0 + 5.75 \log \frac{R'}{2d} \quad (9)$$

where,  $d$  = grain diameter.

Kishi and Kuroki (1973) thought that  $\tau_*$  was a function of  $\tau_*'$  and  $R/d$ . They proposed the relational expressions among  $\tau_* \sim \tau_*' \sim R/d$  in each bed configurations by the data of the experimental channels.

Wang and White (1993) proposed the relational expressions among  $\tau_* \sim \tau_*' \sim D_*$  by the data of the alluvial rivers.

$$D_* = d_{50} \left( \frac{gs}{\nu^2} \right)^{1/3} \quad (9)$$

where,  $s$  = specific gravity of sediment,  $\nu$  = kinematic viscosity.

### 5.2 The resistance of sand waves in the Ishikari River during August 1981 flood

The peak discharge of the August 1981 flood in the Ishikari River exceeded the design discharge. During the flood, the longitudinal bed forms were surveyed (Takagi et al., 1982). The bed configuration changed from Transition to Dune in the flood falling period.

Figure 28 shows the comparison of the relations between  $\tau_*$  and  $\tau_*'$  of the equations of Kishi and Kuroki ( $R/d = 25,000$ ), the curve of Wang and White ( $D_* = 4.75$ ,  $d = 0.19$  mm) with those in 2.5 km upstream from the Ishikari River mouth ( $D_* = 7.6$ ,  $d = 0.3$  mm). Because a large bed scouring occurred in the Ishikari River mouth during the flood, the  $\tau_*$  and  $\tau_*'$  are obtained from the quasi-three dimensional unsteady flood flow and bed variation analysis based on the temporal changes in observed water surface profiles (Okamura and Fukuoka, 2012).

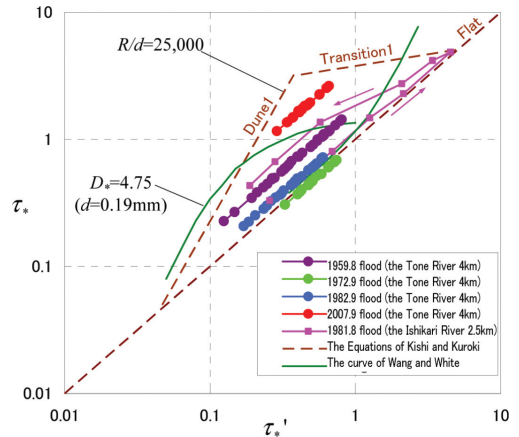


Figure 28. Relations between  $\tau_*$  and  $\tau_*'$  in the Tone River mouth.

The relations between  $\tau_*$  and  $\tau_*'$  in the flood rising period correspond to the Flat bed. On the other hand, the degrees of  $\tau_*$  in the flood falling period are relatively large than those in the flood rising period. They are thought to be the resistance of the dunes surveyed in the flood falling period.

The degrees of the resistance of dunes are smaller than those of the equations of Kishi and Kuroki basing on the data of the steady flow experiments. The sand waves might not develop enough in the Ishikari River because of time lag due to unsteadiness of the flood. On the other hand, the curve of Wang and White basing on the data in the alluvial rivers corresponds with the  $\tau_* \sim \tau_*'$  relation in the Ishikari River.

### 5.3 The resistance of sand waves in the Tone River mouth during the floods

Figure 28 shows the relations between  $\tau_*$  and  $\tau_*'$  in 4.0 km upstream from the Tone River mouth ( $D_* = 4.3$ ,  $d = 0.17$  mm) calculated by the unsteady flood flow and bed variation analysis basing on the temporal changes in observed water surface profiles comparing with the equations of Kishi and Kuroki ( $R/d = 25,000$ ) and the curve of Wang and White ( $D_* = 4.75$ ,  $d = 0.19$  mm).

The resistance in the Tone River during the August 1959 flood is comparable to that in the Ishikari River. But, the value of  $\tau_*$  is equal to  $\tau_*'$  (it means Flat bed) in the September 1972 flood which occurred after most of sand waves disappeared. After that, the resistance increases in a series of floods from 1981 to 1983 when the sand waves grew again. Then the resistance during the September 2007 flood when the height and the distribution area of the sand waves have grown up became larger than the curve of Wang and White and smaller than the equations of Kishi and Kuroki.

There are little changes in the ratios between  $\tau_*$  and  $\tau_*'$  during a flood in the Tone River mouth. They change with the long-term growth and decay of sand waves.

## 6 CONCLUSION

Main conclusions are drawn as follows.

1. It is found that the sand waves are dunes by surveying in the Tone River mouth. We examined the arrangement of dunes which are seen in the downstream of the Choshi Ohashi Bridge located in the reach 2.0 km upstream from the river mouth and verified it to be scale-like dunes as Kinoshita found out.

2. The long-term growing and decaying processes of dunes are indicated by the consideration of variation of cross-sectional bed forms surveyed from 1961 to 2007.
3. We apply the flood flow and sediment movement analysis system based on the observation of temporal changes in water surface profiles to many floods of the Tone River. The variation of sand wave resistances and bed elevations during the floods in different years is evaluated by a numerical analysis of quasi-three dimensional unsteady flood flow and bed variation based on the observed temporal changes in water surface profiles. It is clarified that the degrees of sand wave resistances during floods have changed with the long-term growing and decaying processes of sand waves.
4. The sand wave resistance in the Tone River mouth is featured by comparing with the previous studies on sand wave resistances in alluvial rivers.

## REFERENCES

- Einstein, H.A. and Barbarossa, N.L. (1952) River channel roughness. *Transactions, ASCE*, Vol. 117, 1121–1146.
- Engelund, F. (1967) Closure to “Hydraulic resistance of alluvial streams”. *Journal of the Hydraulics Division, ASCE*, Vol. 93, HY.4, 287–297.
- Fukuoka, S. (2010) River engineering adaptations against the global warming—Towards generalization of close-to-nature rivers. *Proceedings of the Japan Society of Civil Engineers*, F, Vol. 66, No. 4, 471–489, JSCE.
- Fukuoka, S. (2011) What is the fundamentals of river design—Utilization of visible techniques of sediment laden-flood flows. *Advances in River Engineering*, Vol. 17, 83–88, JSCE.
- Fukuoka, S., Watanabe, A. and Okada, S. (1998) Bed topography analysis in a compound meandering channel by using 3D numerical model with approximation of hydrostatics pressure. *Annual Journal of Hydraulic Engineering*, Vol. 42, 1015–1020, JSCE.
- Itakura, T. and Kishi, T. (1980) Open channel flow with suspended sediments. *Journal of Hydraulics Division, Proceedings of ASCE*, Vol. 106, HY.8, 1325–1343.
- Kinoshita, R. (1984) Present status and future prospects of river flow analysis by the aerial photograph. *Proceedings of the Japan Society of Civil Engineers*, Vol. 345/II-1, 1–19, JSCE.
- Kishi, T. and Kuroki, M. (1972) Bed forms and resistance to flow in erodible-bed channels (I), *Bulletin of the Faculty of Engineering Hokkaido University*, Vol. 67.
- Moro, Y., Kazama, S. and Fukuoka, S. (2011) Change of river improvement works of the lower Tone River and effectiveness of channel dredging. *Advances in River Engineering*, Vol. 17, 101–106, JSCE.
- Okamura, S. and Fukuoka, S. (2012) Numerical analysis of unsteady flow and bed variation using temporal changes in water surface profiles during 1981 flood of the Ishikari River mouth. *Proceedings of 3rd ISSF*, Vol. 3.

- Takagi, J., Makino, N., Takemoto, N. and Morita, Y. (1982) Field survey of flood flow and bed evolution in the lower Ishikari River. *Annual Journal of Hydraulic Engineering*, Vol. 26, 57–62, JSCE.
- Uchida, T. and Fukuoka, S. (2009) A depth integrated model for 3D turbulence flows using shallow water equations and horizontal vorticity equations. *33rd IAHR Congress, Water Engineering for a Sustainable Environment*, 1428–1435.
- Wang, S. and White, W.R. (1993) Alluvial resistance in transition regime, *Journal of the Hydraulic Engineering, ASCE*, Vol. 119, No. 6, 725–741.